# Bifurcation mechanism for emergence of spontaneous oscillations in coupled heterogeneous excitable units

Kai Morino,[1,2] Gouhei Tanaka,[1,2,3] and Kazuyuki Aihara[1,2,3,4]

[1]*Graduate School of Information Science and Technology, The University of Tokyo, Tokyo 113-8656, Japan*

[2]*Institute of Industrial Science, The University of Tokyo, Tokyo 153-8505, Japan*

[3]*Graduate School of Engineering, The University of Tokyo, Tokyo 113-8656, Japan*

[4]*International Research Center for Neurointelligence (WPI-IRCN), The University of Tokyo, Tokyo 113-0033, Japan*

(Received 29 May 2018; published 9 November 2018)

Biological systems are often composed of various heterogeneous excitable units. It is a fascinating problem to investigate how this heterogeneity affects collective behavior of biological systems. In this paper, to understand the effect of the unit heterogeneity on the dynamical mechanism for the onset of collective oscillatory behavior, we analyze coupled heterogeneous excitable units. We clarify how spontaneous oscillations emerge depending on the degree of heterogeneity of the units. With an increase in the coupling strength, the system undergoes a saddle-node on invariant circle bifurcation and a heteroclinic bifurcation. Based on bifurcation theory, we reveal that the order of the two bifurcations plays key roles in the mechanism of the emergence of spontaneous oscillations. In addition, we analytically show that when the system has a symmetric property, a 5th-order pitchfork bifurcation occurs instead of the two bifurcations. We also find that spontaneous oscillations are more likely to occur when the sizes of subpopulations of excitable units with different parameters are more balanced.

DOI: 10.1103/PhysRevE.98.052210

## I. INTRODUCTION

There are many physical, chemical, engineering, and biological systems that show *excitability* [1–14]. A dynamical system possessing excitability, called an *excitable system*, settles in a quiescent state when it is not stimulated. When an excitable system is stimulated by a temporal input with a sufficient strength, the state of the system is changed from a quiescent to an excited state. This is followed by a return to the quiescent state after a certain time period. In physics, coupled excitable systems have been analyzed in many studies [1–11]. In chemical systems, the Belousov-Zhabotinsky reaction shows excitable behavior [12]. Traveling waves observed in excitable systems have been extensively studied [13]. In engineering systems, the van der Pol oscillator is a kind of excitable system that originates from specific electronic circuits [14]. In this way, excitability is one of the fundamental properties in real-world systems.

Many biological systems such as neurons and cardiac cells also possess excitability. In the case of neural systems, without a current injection, the membrane potential of a neuron stays at a resting state (called *resting potential*). When the neuron receives a current injection, its membrane potential gradually rises due to accumulation of the injected current. If the membrane potential becomes greater than a threshold value, the neuron generates a spike and the membrane potential returns to the resting state after a refractory period. This excitable behavior has been replicated in mathematical models such as the FitzHugh-Nagumo model [15,16] and the theta neuron model [17]. To understand the dynamic behavior of neuronal systems, the collective behavior of excitable units with identical properties has been studied [5,6,8–11,17]. A next step is to investigate the collective behavior of heterogeneous excitable units, because the brain consists of a wide variety of neurons which are highly heterogeneous. As for cardiac systems, Kryukov *et al.* [18] analyzed a model of a cardiac cell culture consisting of heterogeneous cells in the heart. They combined three types of cell models with different resting potentials. Thus, in this paper, we study the effect of heterogeneous resting potentials (i.e., equilibrium states) of excitable units on collective behavior. A fundamental understanding of the collective behavior of heterogeneous excitable units contributes to a deeper theoretical understanding of biological systems.

The collective behavior of coupled dynamical systems, such as synchronization of coupled oscillators, has been extensively studied [19–22]. Based on the coupled-oscillators theory, the robustness of dynamical systems composed of self-oscillatory (active) units and non-self-oscillatory (inactive) units has also been intensively analyzed in recent years [23–35]. If the proportion of active units is greater than a certain threshold value, global oscillations are observed. Similar transitions occur in a coupled system of other types of units, including excitable and oscillatory ones [1–4]. These results raise a novel issue of whether and how global oscillations emerge in coupled heterogeneous excitable units, without oscillatory units. This question is the other motivation of this study and our aim is to answer this question.

In this paper, we clarify how heterogeneity of excitable units affects their collective behavior. An excitable system can be characterized by the type and position of equilibrium states as well as the threshold corresponding to the basin of attraction of the equilibrium state. It should be reasonable that heterogeneity of these characteristics influences collective behavior of coupled excitable systems. However, as far as

 

we know, collective behavior of heterogeneous excitable units is not fully understood. In this study, we employ a simple excitable model as a unit to understand the mechanism of spontaneous oscillations in coupled heterogeneous excitable units. We find that spontaneous oscillations emerge in coupled excitable units under a certain condition of heterogeneity. We analyze the dynamical mechanism of the onset of spontaneous oscillations based on the bifurcation theory and the center manifold theory. Our results reveal that both local and global bifurcations play important roles in the emergence of spontaneous oscillations.

In the rest of this paper, Sec. II introduces the model of excitable units. Section III shows the bifurcation mechanism for the emergence of spontaneous oscillations in a group of balanced subpopulations. Section IV discusses the spontaneous oscillations in a group of unbalanced subpopulations. In Sec. V, we conclude our study and discuss related future investigations.

## II. MODEL: COUPLED EXCITABLE UNITS

We introduce a phase model that shows excitability, described as follows [1]:

$$\dot{\theta}(t) = 1 - \beta \sin[\theta(t) + a], \tag{1}$$

where $\theta(t)$ is the phase variable at time $t$, $\dot{\theta}(t)$ is the time derivative of $\theta(t)$, $\beta$ indicates the excitability of the model, and $a$ indicates the phase shift which is the factor of the heterogeneity considered in this study. The parameter ranges are given by $\beta \geqslant 0$ and $a \in [0, 2\pi)$. This model shows *self-oscillatory* or *excitable* behavior depending on the value of $\beta$ as shown in Fig. 1. First, we assume that there is no phase shift, i.e., $a = 0$. If $\beta > 1$, this model shows an excitable state; i.e., there is a stable equilibrium point at $\theta = \arcsin(1/\beta)$ and an unstable one at $\theta = \pi - \arcsin(1/\beta)$ [Fig. 1(a)]. At the critical point $\beta = 1$, a *saddle-node on invariant circle* (SNIC) bifurcation occurs [Fig. 1(b)] due to a collision between the stable and unstable equilibrium points. If $0 \leqslant \beta < 1$, this model shows self-oscillatory behavior because there is no equilibrium point [Fig. 1(c)]. The phase shift parameter $a$ does not affect the excitability, but changes the positions of the equilibria [Fig. 1(d)].

We consider a coupled system consisting of $N$ excitable units, described as follows:

$$\dot{\theta}_j = 1 - \beta_j \sin(\theta_j + a_j) + \frac{K}{N}\sum_{k=1}^{N} \sin(\theta_k - \theta_j),$$
$$\text{for } j = 1, \ldots, N, \tag{2}$$

where the last term represents diffusive couplings and $K$ is the coupling strength. This type of coupling, often found in related studies [1], is considered because the phase difference in the steady states is directly influenced by the degree of the unit heterogeneity which we are mainly focusing on in this paper. For simplicity, we assume that all the units are excitable and all the excitability parameters $\beta_j$ are the same as $\beta(>1)$.

Moreover, to discuss how the difference in the positions of the equilibrium states affects the emergence of spontaneous oscillations, we consider two groups with different values of $a_j$. The $N$ units are divided into two groups, for which the

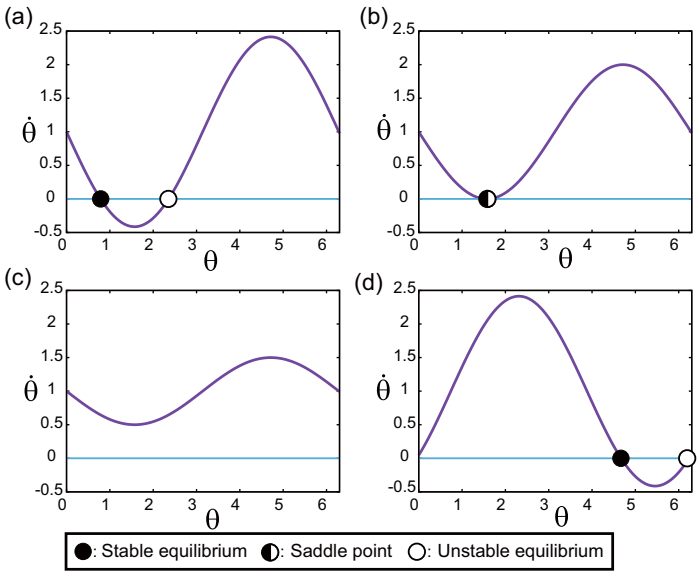


FIG. 1. (a)–(c) Phase portrait of $(\theta, \dot{\theta})$ of the isolated phase model in Eq. (1) with $a = 0$. Parameter $\beta$ is set at (a) $\sqrt{2}$, (b) 1, and (c) 0.5. (a) A stable equilibrium and an unstable one exist if $\beta > 1$. (b) The two equilibria collide at $\beta = 1$ which shows a saddle point. (c) There is no equilibrium if $0 \leqslant \beta < 1$. (d) Phase portrait of $(\theta, \dot{\theta})$ of the isolated phase model in Eq. (1) with $a = 2.4$ and $\beta = \sqrt{2}$. This heterogeneous unit possesses a stable equilibrium and an unstable one whose positions are different from those for $a = 0$ in (a). The horizontal line indicates $\dot{\theta} = 0$.

sets of unit indices are denoted by $S_1$ and $S_2$, respectively. We set $a_j = \alpha_m$ for $j \in S_m$ $(m = 1, 2)$. We express this mapping from the unit index to the group index as $\sigma(j) = m$ $(m = 1, 2)$. Under this assumption, Eq. (2) is rewritten as follows:

$$\dot{\theta}_j = 1 - \beta \sin(\theta_j + \alpha_{\sigma(j)}) + \frac{K}{N}\sum_{k=1}^{N} \sin(\theta_k - \theta_j). \tag{3}$$

Using the new variables, $\hat{\theta}_j := \theta_j + \alpha_1$ and $\alpha := -\alpha_1 + \alpha_2$, Eq. (3) is rewritten as follows:

$$\dot{\hat{\theta}}_j = \begin{cases} f_1(\hat{\theta}_j) + \frac{K}{N}\sum_{k=1}^{N} \sin(\hat{\theta}_k - \hat{\theta}_j), & \text{if } j \in S_1, \\ f_2(\hat{\theta}_j, \alpha) + \frac{K}{N}\sum_{k=1}^{N} \sin(\hat{\theta}_k - \hat{\theta}_j), & \text{if } j \in S_2, \end{cases} \tag{4}$$

where $f_1(\hat{\theta}) := 1 - \beta \sin(\hat{\theta})$ and $f_2(\hat{\theta}, \alpha) := 1 - \beta \sin(\hat{\theta} + \alpha)$. From our numerical simulations, it is confirmed that the phases of the units within the same group synchronize (not shown). Thus, hereafter, we assume that $\hat{\theta}_j = \phi_1$ for $j \in S_1$ and $\hat{\theta}_j = \phi_2$ for $j \in S_2$. This approach is the same as that of the previous study [36]. Then, Eq. (4) can be reduced to a two-unit system as follows:

$$\dot{\phi}_1 = 1 - \beta \sin(\phi_1) + qK \sin(\phi_2 - \phi_1), \tag{5}$$

$$\dot{\phi}_2 = 1 - \beta \sin(\phi_2 + \alpha) + (1 - q)K \sin(\phi_1 - \phi_2), \tag{6}$$

where $q$ is the proportion of the units belonging to $S_2$. We define a *balanced population* as the case of $q = 1/2$ and an *unbalanced population* as the case of $q \neq 1/2$. Note that there are four parameters $\alpha \in [0, 2\pi)$, $\beta > 1$, $K \geqslant 0$, and $q \in [0, 1]$ in the above model. Later, we analyze this

two-unit model and validate the result by brute-force numerical simulations.

The frequency of $\phi_j$ $(j = 1, 2)$, or the velocity of the phase, is defined as follows:

$$\Omega_j := \lim_{T\to\infty} \frac{1}{T} \int_{t=t_0}^{t_0+T} \dot{\phi}_j(t)\, dt = \lim_{T\to\infty} \frac{\phi_j(t_0+T) - \phi_j(t_0)}{T}, \tag{7}$$

where $t_0$ is a time point corresponding to the end of the transient period. When $\Omega_j$ is positive, the phase of the corresponding unit increases over time. On the contrary, when $\Omega_j$ is zero, the state of the unit does not rotate on the unit circle. For the numerical simulation, we employed the fourth-order Runge-Kutta method with time step $\Delta t$ ($\Delta t \leqslant 0.01$).

We note that there is no need to analyze the entire parameter space because two symmetric properties exist in our system. We summarize the details of the two symmetries in Appendix A. From these symmetries, we can restrict the parameter region of $(\alpha, q)$ to be analyzed to $\{(\alpha, q) \mid \alpha \in [\pi/2, 3\pi/2], q \in [1/2, 1]\}$. In this region, we found interesting bifurcations which will be introduced in the later sections. In addition, we can understand the dynamics for other regions on the $(\alpha, q)$ plane based on the two symmetric properties. Thus, later, we will focus mainly on this parameter region.

Throughout this paper, we focus on the heterogeneity of $a_j$. However, we note that heterogeneity of $\beta_j$ is also of significant interest. Because the parameter $\beta_j$ directly controls the qualitative behavior of the model, the heterogeneity of $\beta_j$ generates a mix of oscillatory and excitable units [1–4]. Thus, the system containing dual heterogeneity of $a_j$ and $\beta_j$ may show rich and interesting behavior, and should be discussed in future.

Finally, we briefly mention the relationship between our models and previous studies. A model of excitable phase oscillator can be derived from the Kuramoto model using an order parameter [37,38]. A phase model similar to our model has been studied in relation to the Kuramoto model with external forcing [38–42], active rotators [43,44], and models of charge density wave [45–47]. See Appendix B for detailed information on this relationship.

## III. BALANCED POPULATIONS

In this section, we focus on how the heterogeneity parameter $\alpha$ affects the emergence of spontaneous oscillations in the balanced population case of $q = 1/2$, where the numbers of units in the two groups are the same. With an increase in the coupling strength $K$, two types of spontaneous oscillations emerge. We reveal that the type is determined depending on the order of occurrence of the SNIC and heteroclinic bifurcations in the case of $\alpha \neq \pi$. In Sec. III A, we introduce the model for $q = 1/2$. We discuss the individual emergence for $\alpha \in (\alpha_*, \pi)$ in Sec. III B and the simultaneous emergence for $\alpha \in (\pi/2, \alpha_*)$ in Sec. III C. We note that $\alpha_*$ is the boundary between these two cases and is introduced later. We reveal that a pitchfork bifurcation is responsible for the emergence of spontaneous oscillation for $\alpha = \pi$ in Sec. III D. Finally, in Sec. III E, we discuss the situations for the remaining range of $\alpha$ based on the symmetric properties of the system.

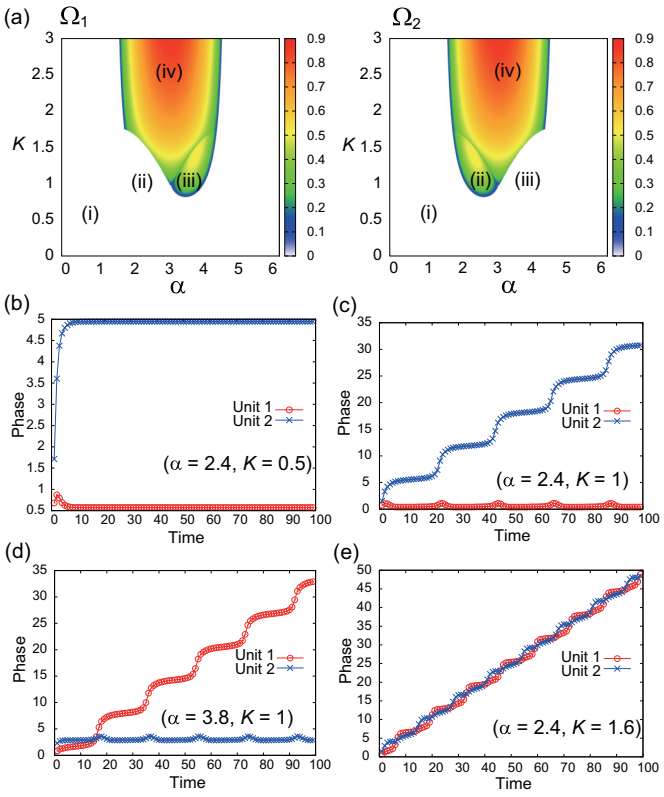


FIG. 2. (a) The parameter region for spontaneous oscillations. The frequencies $\Omega_1$ (left) and $\Omega_2$ (right) are indicated by the color on the parameter plane $(\alpha, K)$. The planes are divided into four specific regions: (i) $\Omega_1 = \Omega_2 = 0$, (ii) $\Omega_1 = 0$ and $\Omega_2 > 0$, (iii) $\Omega_1 > 0$ and $\Omega_2 = 0$, and (iv) $\Omega_1 = \Omega_2 > 0$. (b)–(e) Time evolutions of the phase variables, $\phi_1$ and $\phi_2$, are shown for $(\alpha, K) =$ (b) $(2.4, 0.5)$, (c) $(2.4, 1)$, (d) $(3.8, 1)$, and (e) $(2.4, 1.6)$. These panels (b)–(e) correspond to the cases (i)–(iv) in panel (a), respectively. The other parameter values are set at $\beta = \sqrt{2}$ and $q = 1/2$ for all the cases.

### A. Model

In the case of $q = 1/2$, the system is rewritten from Eqs. (5) and (6) as follows:

$$\dot{\phi}_1 = 1 - \beta \sin(\phi_1) + \frac{K}{2} \sin(\phi_2 - \phi_1), \tag{8}$$

$$\dot{\phi}_2 = 1 - \beta \sin(\phi_2 + \alpha) + \frac{K}{2} \sin(\phi_1 - \phi_2). \tag{9}$$

When they are isolated ($K = 0$), there is a stable equilibrium point at $(\phi_1^*, \phi_2^*) = (\arcsin(1/\beta), \arcsin(1/\beta) - \alpha)$, two saddle points, and an unstable equilibrium point in the region of $(\phi_1, \phi_2) \in [0, 2\pi) \times [0, 2\pi)$. With an increase in $K$ from 0, spontaneous oscillations occur under a certain condition of parameter $\alpha$. We show the frequencies $\Omega_1$ and $\Omega_2$ on the $(\alpha, K)$ plane for $\beta = \sqrt{2}$ in Fig. 2(a). The parameter region can be divided into four parts: (i) $\Omega_1 = \Omega_2 = 0$; (ii) $\Omega_1 = 0$ and $\Omega_2 > 0$; (iii) $\Omega_1 > 0$ and $\Omega_2 = 0$; (iv) $\Omega_1 = \Omega_2 > 0$. We show the time series of $\phi_1$ and $\phi_2$ for four values of $K$ in Figs. 2(b)–2(e), which correspond to (i)–(iv), respectively. We

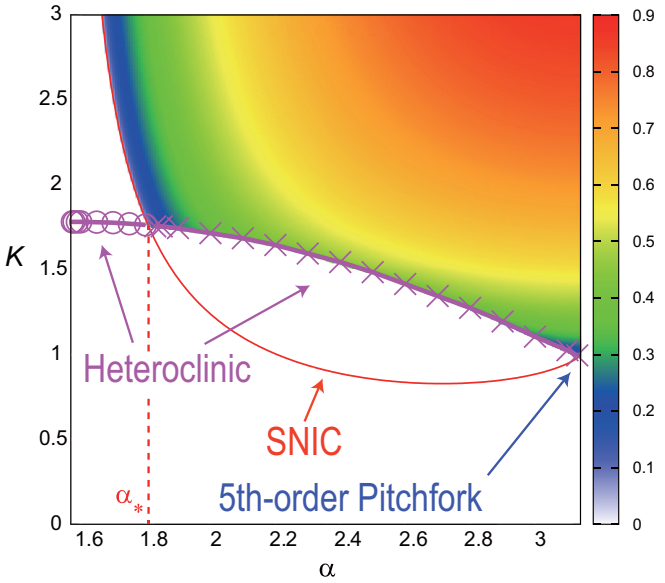


FIG. 3. Bifurcation diagram showing the mechanism of the emergence of spontaneous oscillations. This figure is an enlargement of the $\Omega_1$ part of Fig. 2(a). We set $\beta = \sqrt{2}$. The red curve indicates the parameter set where the SNIC bifurcation occurs. The purple curve indicates the parameter set where the heteroclinic bifurcation occurs. We indicate $\alpha_*$ by the dashed line.

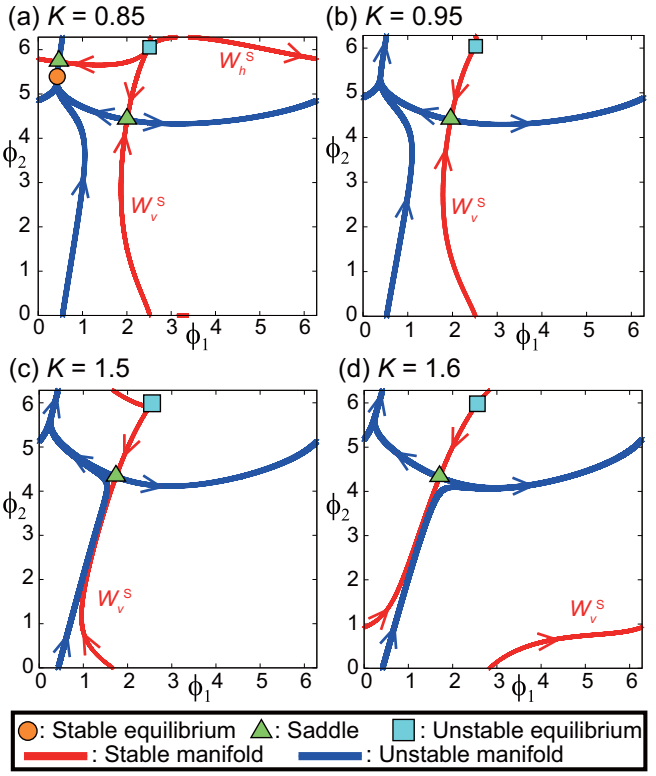


FIG. 4. Phase portrait on the $(\phi_1, \phi_2)$ plane for $\alpha = 2.4$ and $\beta = \sqrt{2}$. The coupling strength $K$ is set at (a) 0.85, (b) 0.95, (c) 1.5, and (d) 1.6. The SNIC bifurcation occurs between (a) and (b), where the upper-left saddle point and the stable equilibrium point collide with each other. The heteroclinic bifurcation occurs between (c) and (d). Arrows shown on the manifolds indicate the direction of orbits on the manifolds.

note that Fig. 2 shows the results obtained from the numerical simulation of Eqs. (8) and (9).

Two types of bifurcation occur with an increase in $K$: heteroclinic bifurcation which is a global bifurcation and SNIC bifurcation which is a local bifurcation. For $\alpha \in (\pi/2, \pi)$, with an increase in $K$ from 0, the stable equilibrium point vanishes through a SNIC bifurcation at a critical point $K = K_*(\alpha)$. The system shows spontaneous oscillatory behavior for $K > K_*(\alpha)$. Figure 3 is an enlargement of a part of Fig. 2(a), showing the color-coded value of $\Omega_1$ and the curve for $K_*(\alpha)$ on the $(\alpha, K)$ plane for $\beta = \sqrt{2}$. It is clear that there are two types of scenarios after the SNIC bifurcation occurs. For $\alpha < \alpha_* \sim 1.808$, both $\phi_1$ and $\phi_2$ start to increase simultaneously at the SNIC bifurcation point. For $\alpha > \alpha_*$, only $\phi_2$ starts to increase at the SNIC bifurcation and then after the heteroclinic bifurcation, $\phi_1$ starts to increase as well. We note that $\alpha_*$ corresponds to the intersection of the SNIC and heteroclinic bifurcation curves as shown in Fig. 3. In the following subsections, we show the details of the two bifurcation scenarios in Secs. III B and III C and a special case in Sec. III D.

### B. Individual emergence of spontaneous oscillations

For $\alpha \in (\alpha_*, \pi)$, only $\phi_2$ begins to increase just after the SNIC bifurcation. The other unit of $\phi_1$ needs a larger value of $K$ to exhibit oscillations as shown in Figs. 2 and 3. This sequential emergence of oscillations can be understood based on the dynamical mechanism as shown in Fig. 4. We call this type of emergence "*individual emergence*" of oscillations in this paper. We note that a small region, where $\alpha$ is very close to $\pi$, shows hysteresis phenomena. This phenomenon is observed in other related models [45–47] as discussed in Appendix B.

Figure 4 shows the phase portrait on the $(\phi_1, \phi_2)$ plane for $\alpha = 2.4$ before and after the two bifurcations. The red curves indicate the stable manifolds that connect a saddle point and the unstable equilibrium point. The blue curves indicate the unstable manifolds that connect a saddle point and the stable equilibrium point. When the stable equilibrium point and stable manifolds exist, orbits converge to the stable equilibrium point. Note that this figure contains only the information that is related to the emergence of spontaneous oscillations. Hereafter, we denote the stable manifold that vertically stretches along the $\phi_2$ axis by $W_v^S$ and that horizontally stretches along the $\phi_1$ axis by $W_h^S$.

Figures 4(a) and 4(b) show the phase portraits on the $(\phi_1, \phi_2)$ plane before and after the SNIC bifurcation at $K \sim 0.888$, respectively. As shown in these two figures, the stable point, the upper-left saddle point, and the horizontal stable manifold $W_h^S$ vanishes via the SNIC bifurcation, while the vertical stable manifold $W_v^S$ remains. Because orbits cannot cross $W_v^S$, they cannot rotate in the direction of $\phi_1$ but can in the direction of $\phi_2$. This is the reason why $\Omega_1 = 0$ and $\Omega_2 > 0$ after the SNIC bifurcation.

Figures 4(c) and 4(d) show the phase portraits before and after the heteroclinic bifurcation at $K \sim 1.54$, respectively.

The vertical stable and unstable manifolds become closer as $K$ gets closer to the heteroclinic bifurcation point, and they collide with each other. After the heteroclinic bifurcation, the stable manifold $W_v^S$ is changed to have an intersection with the line $\phi_1 = 0$. This change makes it possible that the orbit can reach the next right region without crossing the stable manifold. We note that the system has $2\pi$ periodicity for both $\phi_1$ and $\phi_2$. This is the reason why both units can oscillate after the heteroclinic bifurcation.

We mention the numerical method used to obtain these manifolds that connect to the saddle points. The stable manifolds correspond to the basin boundaries of the stable equilibrium points. Therefore, we compute the basin boundaries of the stable equilibria. The unstable manifolds can be obtained by simulating the model backward in time because they correspond to the basin boundaries of the stable equilibria of the time-inverse system.

### C. Simultaneous emergence of spontaneous oscillations

Contrary to the previous scenario, for $\alpha \in [\pi/2, \alpha_*)$, both the units of $\phi_1$ and $\phi_2$ start to oscillate simultaneously at $K = K_*(\alpha)$. We call this type of emergence "*simultaneous emergence*" of oscillations in this paper. As shown in Fig. 3, the difference between the two scenarios is the order of occurrence of the SNIC and the heteroclinic bifurcations. In this subsection, we show why the simultaneous emergence of spontaneous oscillation is caused when the heteroclinic bifurcation is followed by the SNIC one. Figure 5 shows the phase portrait on the $(\phi_1, \phi_2)$ plane before and after the two bifurcations for $\alpha = 1.7$.

Figures 5(a) and 5(b) show the phase portraits before and after the heteroclinic bifurcation at $K \sim 1.777$, respectively. Similarly to the case in the previous subsection, the vertical stable and unstable manifolds become closer to each other as $K$ gets closer to the heteroclinic bifurcation point and they collide with each other. Then, this stable manifold is changed to have an intersection with the line $\phi_1 = 0$. The stable equilibrium point remains after this heteroclinic bifurcation and therefore orbits starting from any initial conditions finally converge to the stable equilibrium point. Thus, this heteroclinic bifurcation cannot trigger spontaneous oscillations.

A further increase in $K$ results in the initiation of oscillation in both the units of $\phi_1$ and $\phi_2$ via the SNIC bifurcation. Figures 5(c) and 5(d) show the phase portraits before and after SNIC bifurcation at $K \sim 2.49$, respectively. Both the stable equilibrium point and the lower-left saddle point vanish via this bifurcation, and then, no horizontal stable manifold which blocks a phase slip of the orbits remains. Hence, the orbit can rotate in both directions of $\phi_1$ and $\phi_2$. This is the reason why both units simultaneously start to oscillate after this SNIC bifurcation.

### D. Pitchfork bifurcations for $\alpha = \pi$

In this subsection, we focus on the bifurcation mechanism for $\alpha = \pi$. The system shows a 3rd-order pitchfork bifurcation and a 5th-order pitchfork bifurcation, depending on the symmetric property of the system. We briefly sketch our analysis based on the center manifold theory [48]. A detailed derivation is shown in Appendix C.

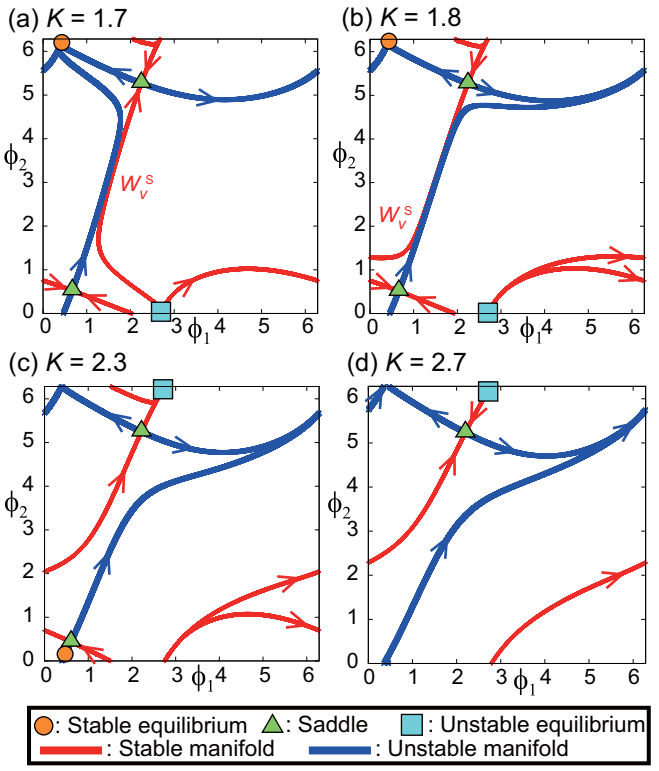


FIG. 5. Phase portrait on the $(\phi_1, \phi_2)$ plane for $\alpha = 1.7$ and $\beta = \sqrt{2}$. The coupling strength $K$ is set at (a) 1.7, (b) 1.8, (c) 2.3, and (d) 2.7. The heteroclinic bifurcation occurs between (a) and (b). The SNIC bifurcation occurs between (c) and (d), where the lower-left saddle point and the stable equilibrium point collide with each other. Arrows shown on the manifolds indicate the direction of orbits on the manifolds.

First, we obtain the dynamics on the center manifold. For $\alpha = \pi$, Eqs. (5) and (6) have an equilibrium point at $(\phi_1^*, \phi_2^*) = (\arcsin(1/\beta), \arcsin(1/\beta) + \pi)$. We denote the displacement from the equilibrium point by $(\psi_1, \psi_2) := (\phi_1 - \phi_1^*, \phi_2 - \phi_2^*)$. By substituting these equations into Eqs. (5) and (6), the linear part of the time expansion equation of the displacement $(\psi_1, \psi_2)$ is given in the following form:

$$\begin{pmatrix} \dot{\psi}_1 \\ \dot{\psi}_2 \end{pmatrix} = A \begin{pmatrix} \psi_1 \\ \psi_2 \end{pmatrix}, \tag{10}$$

where

$$A = \begin{pmatrix} -\sqrt{\beta^2 - 1} + Kq & -Kq \\ -K(1-q) & -\sqrt{\beta^2 - 1} + K(1-q) \end{pmatrix}. \tag{11}$$

The two eigenvalues of $A$ are given as $\lambda_K := K - \sqrt{\beta^2 - 1}$ and $\lambda_0 := -\sqrt{\beta^2 - 1} < 0$ and their corresponding eigenvectors are $\mathbf{e}_K = 2(q, q-1)^\top$ and $\mathbf{e}_0 = (1, 1)^\top$, respectively. This indicates that the stability of the equilibrium point changes at $K = \sqrt{\beta^2 - 1}$. We transform the variables from $(\psi_1, \psi_2)$ into $(u, v)$ as follows:

$$\begin{pmatrix} \psi_1 \\ \psi_2 \end{pmatrix} = u\, \mathbf{e}_0 + v\, \mathbf{e}_K, \tag{12}$$

which gives the following relationship:

$$u = (1-q)\psi_1 + q\psi_2, \tag{13}$$

$$v = \frac{\psi_1 - \psi_2}{2}. \tag{14}$$

We note that $\psi_1$ and $\psi_2$ are functions of $u$ and $v$. Equation (12) indicates that $u$ and $v$ correspond to the stable and center manifolds at $K = \sqrt{\beta^2 - 1}$, respectively. According to the center manifold theory [48], on the center manifold, $u$ can be written as a function of $v$ as follows:

$$u = m(v) := \sum_{k \geqslant 2} a_k v^k. \tag{15}$$

The time derivative of Eq. (13) and that of Eq. (15) must agree with each other. From a comparison of the derivatives, we can obtain the reduced system on the center manifold as follows:

$$\dot{v} = (K - \sqrt{\beta^2 - 1})v + \sum_{k \geqslant 2} C_k v^k. \tag{16}$$

As above, we can describe the dynamical behavior in the vicinity of the bifurcation point at $K = \sqrt{\beta^2 - 1}$. Next, we derive how this dynamics depends on $\beta$ and $q$.

#### *1. 3rd-order pitchfork bifurcation*

The coefficient $C_2$ is given by $C_2 = 2q - 1$, and thus, when $q = 1/2$, the coefficient $C_2$ equals zero. Then, Eq. (16) is rewritten as follows:

$$\dot{v} = (K - \sqrt{\beta^2 - 1})v + C_3 v^3 + O(v^4), \tag{17}$$

where $C_3 = \frac{2-\beta^2}{2\sqrt{\beta^2-1}}$. When $C_3 \neq 0$ ($\beta \neq \sqrt{2}$), Eq. (17) can be approximated as a 3rd-order polynomial equation as follows:

$$\dot{v} = (K - \sqrt{\beta^2 - 1})v + C_3 v^3, \tag{18}$$

because the magnitude of $v$ is relatively small. Therefore, the system shows a pitchfork bifurcation at $K = \sqrt{\beta^2 - 1}$: a supercritical pitchfork bifurcation for $C_3 < 0$ ($\beta > \sqrt{2}$) and a subcritical pitchfork bifurcation for $C_3 > 0$ ($\beta < \sqrt{2}$). Using the solution of Eq. (18), the $v$ values at the equilibrium points are given by $v = 0$ and

$$v = \pm\sqrt{-\frac{K - \sqrt{\beta^2 - 1}}{C_3}}. \tag{19}$$

Note that the domain of $K$ depends on the sign of $C_3$ as follows:

$$\begin{aligned} K &\leqslant \sqrt{\beta^2 - 1}, \quad \text{if } C_3 > 0, \\ K &\geqslant \sqrt{\beta^2 - 1}, \quad \text{if } C_3 < 0. \end{aligned} \tag{20}$$

The corresponding $u$ values at the equilibrium points are obtained by $u = a_2 v^2$. By using Eqs. (13) and (14), the original trajectory $(\phi_1, \phi_2)$ is obtained as follows:

$$\begin{aligned} \phi_1 &= u + v + \phi_1^*, \\ \phi_2 &= u - v + \phi_2^*. \end{aligned} \tag{21}$$

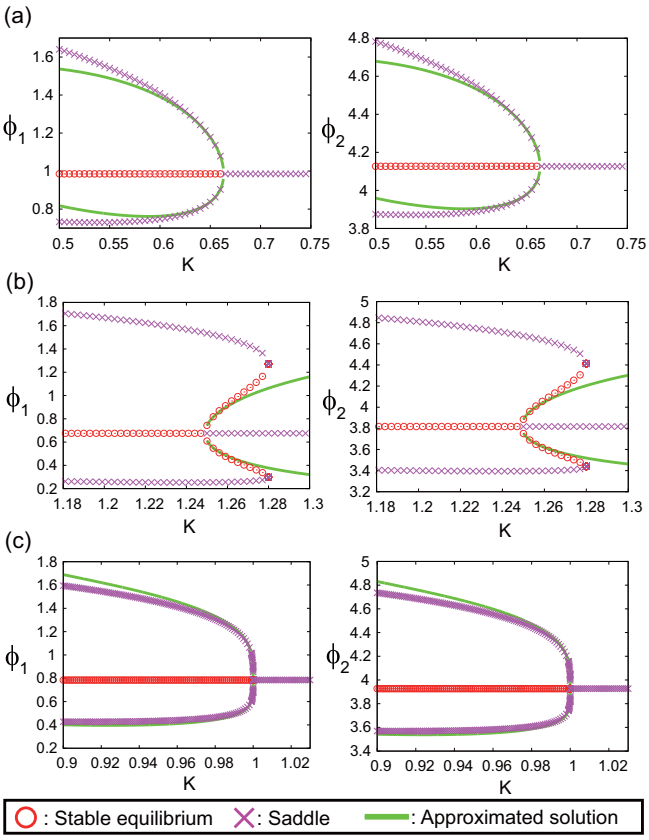


FIG. 6. Bifurcation diagram for a variation of $K$, where $\alpha = \pi$. Stable equilibrium points (red, ○), saddle points (purple, ×), and approximated solution of the bifurcation (green solid curve) are shown. (a) A 3rd-order subcritical pitchfork bifurcation occurs at $K \sim 0.6633$. (b) A 3rd-order supercritical pitchfork bifurcation occurs at $K \sim 1.2490$. (c) A 5th-order subcritical pitchfork bifurcation occurs at $K = 1$. The parameters $(q, \beta)$ are set at (a) (0.5, 1.2), (b) (0.5, 1.6), (c) (0.5, $\sqrt{2}$).

We numerically confirmed that this approximation works well near the bifurcation point $K = \sqrt{\beta^2 - 1}$ as shown in Fig. 6(a) for $\beta = 1.2$ (subcritical) and in Fig. 6(b) for $\beta = 1.6$ (supercritical). In Fig. 6(a), the spontaneous oscillations emerge via the subcritical pitchfork bifurcation. On the contrary, in Fig. 6(b), two stable equilibrium points are generated via the supercritical pitchfork bifurcation, and then, they disappear via the subsequent SNIC bifurcation.

#### *2. 5th-order pitchfork bifurcation*

In the special case where $q = 1/2$ and $\beta = \sqrt{2}$, the coefficients $C_2$, $C_3$, and $C_4$ are equal to zero. In this case, we need to investigate higher order terms of $v$. Equation (16) is rewritten as

$$\dot{v} = (K - \sqrt{\beta^2 - 1})v + C_5 v^5 + O(v^6), \tag{22}$$

where $C_5 = 1/2 > 0$ at $K = \sqrt{\beta^2 - 1} = 1$. Therefore, the system shows a 5th-order subcritical pitchfork bifurcation. Equation (22) can be approximated as a 5th-order-polynomial equation as follows:

$$\dot{v} = (K - \sqrt{\beta^2 - 1})v + C_5 v^5. \tag{23}$$

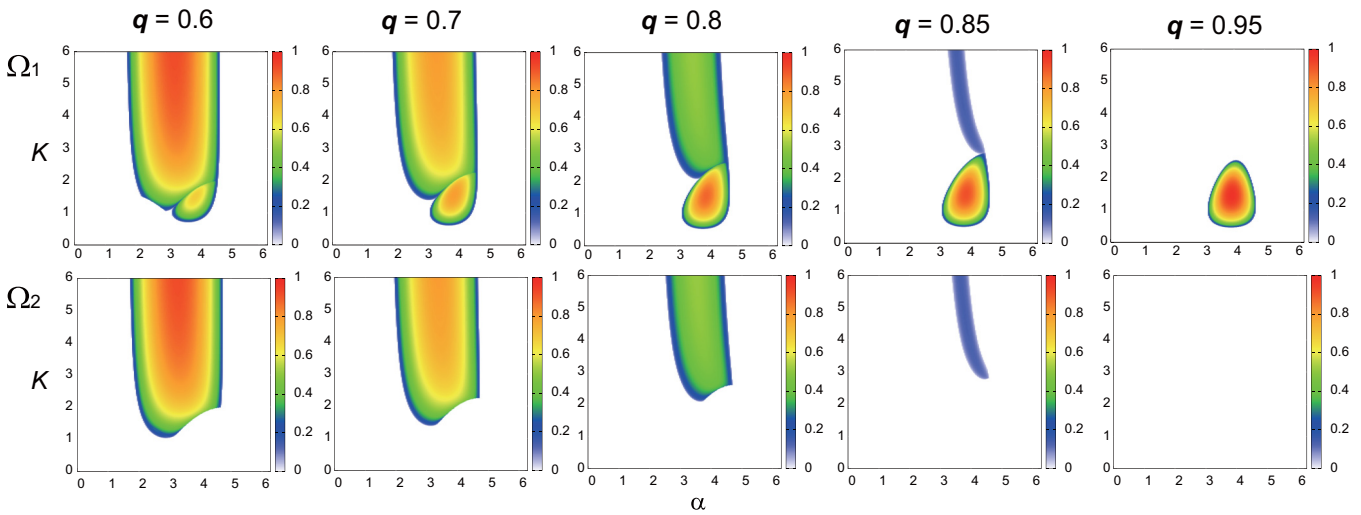


FIG. 7. The parameter region corresponding to spontaneous oscillation depends on $q$. The frequencies $\Omega_1$ (upper) and $\Omega_2$ (lower) are indicated by the color on the parameter plane of $(\alpha, K)$ for $\beta = \sqrt{2}$. The value of $q$ is varied from 0.6 (left) to 0.95 (right).

Using the solution of Eq. (23), the $v$ values at the equilibrium points are given by $v = 0$ and

$$v = \pm\sqrt{\sqrt{-\frac{K-\sqrt{\beta^2-1}}{C_5}}}. \tag{24}$$

The corresponding $u$ values at the equilibrium points are also obtained by $u = a_2 v^2$. By using Eqs. (13) and (14), the original trajectory $(\phi_1, \phi_2)$ is obtained from Eq. (21). We numerically confirmed that this approximation works well near the bifurcation point $K = 1$ as shown in Fig. 6(c). Spontaneous oscillations emerge after this 5th-order subcritical pitchfork bifurcation.

### E. Spontaneous oscillations in the other range of α

From the previous analysis for $\alpha \in [\pi/2, \pi]$, we have clarified how and when the spontaneous oscillations occur depending on the heterogeneity parameter $\alpha$. We can understand the case with the other parameter range of $\alpha$ using the two symmetric properties described in Appendix A. For $\alpha \in [0, \pi/2)$, the system does not exhibit any oscillations. This can be understood from the symmetric property in Eq. (A7). For $\alpha \in [\pi, 2\pi]$, the dynamical behavior of the system can be understood from the symmetric property in Eq. (A1).

In this section, we have discussed the emergence of spontaneous oscillations in the case of balanced populations. In the next section, we will discuss spontaneous oscillations in unbalanced populations.

## IV. UNBALANCED POPULATIONS

Next, we discuss the emergence of spontaneous oscillations in the system of unbalanced populations, i.e., the cases of $q > 1/2$ and $q < 1/2$. We again note that $q$ is the proportion of the units belonging to $S_2$, and the frequencies of $\phi_1$ and $\phi_2$ are denoted by $\Omega_1$ and $\Omega_2$, respectively. In this section, we only consider the case of $q > 1/2$; i.e., $\phi_1$ corresponds to the minority units and $\phi_2$ corresponds to the majority units. Note that the other case can be similarly understood based on the symmetric property. See Appendix A for details.

### A. Individual and simultaneous emergence of spontaneous oscillations

The parameter $q$ affects the dependencies of $\Omega_1$ and $\Omega_2$ on the parameters $\alpha$ and $K$ as shown in the upper and lower panels of Fig. 7, respectively. This result indicates that the minority units are a key factor for maintaining oscillations.

As in the previous cases of the balanced populations, there are two types of emergence of spontaneous oscillations: individual emergence and simultaneous emergence. In the former case, the parameter regions for the spontaneous oscillations are different between the minority units ($\phi_1$) and the majority units ($\phi_2$). The parameter region for spontaneous oscillations tends to slightly increase with $q$ for the minority units, while it dramatically decreases with $q$ for the majority units. In the latter case, the parameter region for simultaneous oscillations tends to decrease with an increase in $q$ for both types of units. The dynamical mechanism of these emergences can be understood by SNIC and heteroclinic bifurcations as shown in Figs. 8(a)–8(c): the SNIC and the heteroclinic bifurcation curves are shown on the $(\alpha, K)$ plane for $q = 0.6$ and 0.85. We can find that the boundaries between $\Omega_1 = 0$ and $\Omega_1 > 0$ (also $\Omega_2 = 0$ and $\Omega_2 > 0$) correspond to the bifurcation curves. This is similar to the case of the balanced populations as shown in Fig. 3.

However, at a certain range of $\alpha$ and $q$, the bifurcation mechanism is more complex than that of the balanced populations ($q = 1/2$). Figures 8(a) and 8(b) indicate that the bifurcation mechanism is the same as that in the previous section except for $\alpha$ in the vicinity of $\pi$; i.e., SNIC and heteroclinic bifurcations occur with an increase in $K$. In the vicinity of $\alpha = \pi$, the bifurcation mechanism is different because bifurcations occur four times for an increase in $K$: one heteroclinic bifurcation and three SNIC bifurcations. The phase planes for understanding these bifurcations are shown in Fig. 9. Figures 9(a) and 9(b) show the phase portraits before

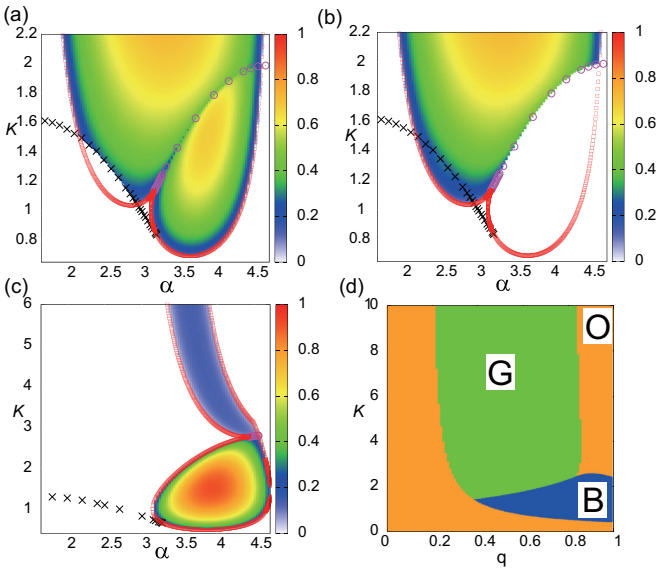


FIG. 8. (a)–(c) Frequencies are plotted on $(\alpha, K)$ plane: (a) $\Omega_1$ for $q = 0.6$; (b) $\Omega_2$ for $q = 0.6$; and (c) $\Omega_1$ for $q = 0.85$. The bifurcation curves for the heteroclinic bifurcations are plotted as purple ○ and black × and those for the SNIC bifurcation are plotted as red □. (d) For the case of $\alpha = 4$, the $(q, K)$ plane is divided into three regions: the green (marked as G), blue (marked as B), and orange (marked as O) regions correspond to the cases where both $\Omega_1$ and $\Omega_2$ are positive, $\Omega_1$ is positive and $\Omega_2$ is zero, and $\Omega_1 = \Omega_2 = 0$, respectively. In all the panels, the $\beta$ is set at $\sqrt{2}$.

and after the heteroclinic bifurcation at $K \sim 0.8905$. The vertical stable manifold $W_v^S$ is changed to have an intersection with $\phi_1 = 0$ as in Fig. 5(b). Figures 9(c) and 9(d) show the phase portraits before and after the first SNIC bifurcation at $K \sim 0.944$. After this first SNIC bifurcation, there remains the horizontal stable manifold $W_h^S$ which is different from the case of Fig. 5(d). This is because the saddle point vanishes via the SNIC bifurcation. A comparison between Figs. 5(c) and 5(d) reveals that the saddle point connecting to $W_h^S$ vanishes. After this first SNIC bifurcation, the saddle point connecting to $W_v^S$ vanishes. Thus, in this situation, spontaneous oscillations individually emerge. Figures 9(e) and 9(f) show the phase portraits before and after the second SNIC bifurcation at $K \sim 1.059$. The stable equilibrium point emerges via this second SNIC bifurcation, and thus, the oscillation vanishes. Figures 9(g) and 9(h) show the phase portraits before and after the third SNIC bifurcation at $K \sim 1.106$. Because the saddle point connecting to $W_h^S$ vanishes via this SNIC bifurcation, spontaneous oscillation simultaneously emerges.

Next, we discuss the effects of $q$ for larger values of $K$. The parameter regions corresponding to spontaneous oscillations decrease with an increase in $q$ as shown in Fig. 7. The coupling terms in Eqs. (5) and (6) can be used to explain this phenomenon. The coupling term of $\phi_2$ (majority units) is $(1 - q)K \sin(\phi_1 - \phi_2)$ which becomes smaller for larger $q$ and that of $\phi_1$ (minority units) is $qK \sin(\phi_2 - \phi_1)$ which becomes larger for larger $q$. Thus, for a larger value of $q$, $\phi_2$ receives weak coupling effects and behaves similarly to its isolated case, but $\phi_1$ receives strong coupling effects. Figure 8(d) indicates three subregions on the $(q, K)$ plane for $\alpha = 4$, which

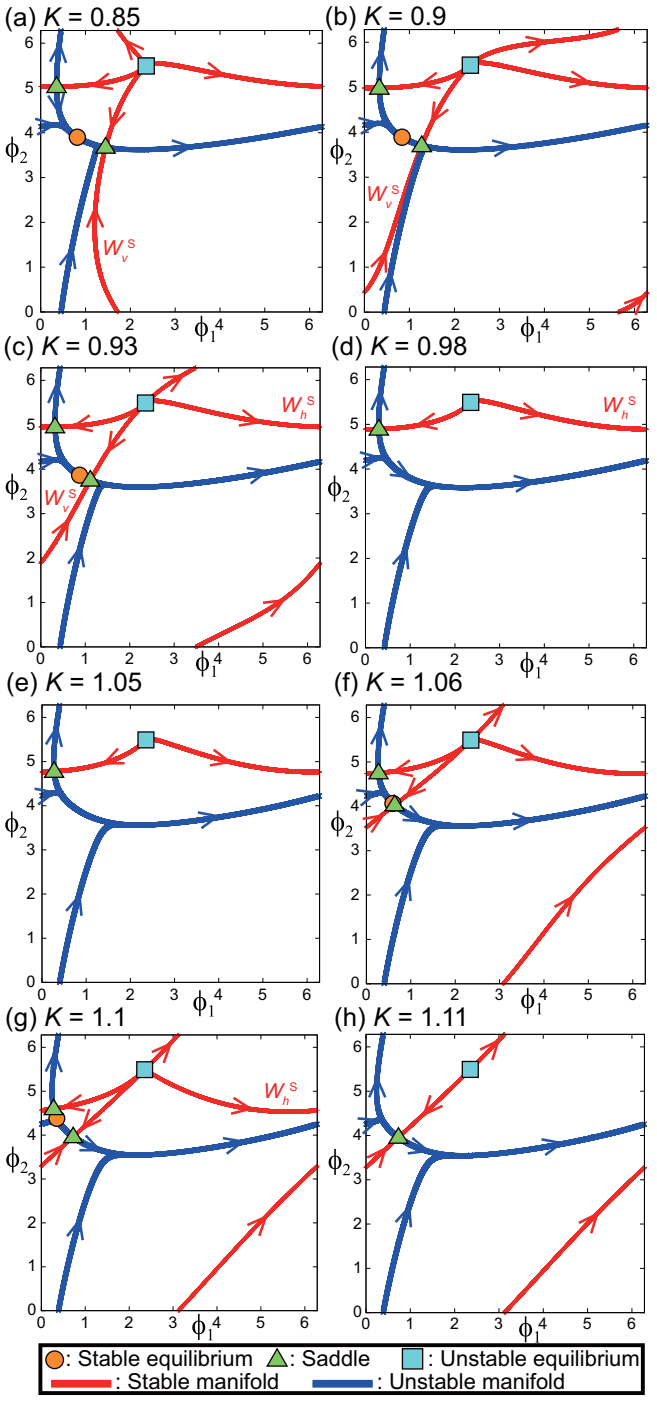


FIG. 9. Phase portrait on the $(\phi_1, \phi_2)$ plane in the case of $\alpha = 3.15$, $q = 0.6$, and $\beta = \sqrt{2}$. The coupling strength $K$ increases from (a) to (h). The heteroclinic bifurcation occurs between (a) and (b). The SNIC bifurcation occurs three times: between (c) and (d); between (e) and (f); and between (g) and (h). Arrows shown on the manifolds indicate the direction of the orbits on the manifolds.

are colored with green, blue, and orange. The green, blue, and orange regions correspond to the cases where both $\Omega_1$ and $\Omega_2$ are positive, $\Omega_1$ is positive and $\Omega_2$ is zero, and $\Omega_1 = \Omega_2 = 0$, respectively. For these three regions, we explain the dynamics after a transient period as follows. In the green region with larger values of $K$ and a slightly unbalanced population

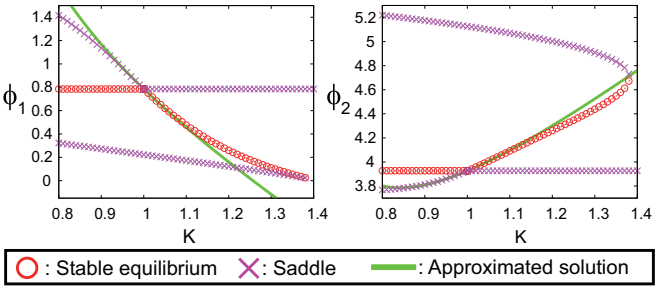


FIG. 10. Bifurcation diagram for a variation of $K$, where $\alpha = \pi$. A transcritical bifurcation occurs at $K = 1$. Stable equilibrium points (red, ○), saddle points (purple, ×), and approximate solution of the bifurcation (green solid curve) are shown. The parameters $(q, \beta)$ are set at $(0.7, \sqrt{2})$.

$(q \in [1/2, q_*]$ $(q_* \sim 0.85))$, all the units oscillate. In the orange region with a highly unbalanced population $(q > q_*)$, all the units do not show oscillation. In the blue region with small $K$, the majority units do not show the spontaneous oscillations (i.e., phase slips) but show fluctuations because they are affected weakly by the oscillations of the minority units. This result reflects the previous discussion: the majority units receive a little coupling effect and behave similarly to its isolated case, i.e., they do not exhibit oscillation (phase slip) for a highly unbalanced population; the minority units experience significant coupling effects, i.e., they are entrained into the majority units for large coupling strength. Thus, the parameter regions corresponding to spontaneous oscillations decrease with an increase in $q$.

### B. Transcritical bifurcation for $\alpha = \pi$

In the special case where $\alpha = \pi$ and $q \neq 1/2$, a transcritical bifurcation occurs. As we have discussed in Sec. III D, for $\alpha = \pi$, Eqs. (5) and (6) have an equilibrium point at $(\phi_1^*, \phi_2^*) = (\arcsin(1/\beta), \arcsin(1/\beta) + \pi)$. Based on the center manifold theory, we can reveal the bifurcation mechanism for this equilibrium point using Eq. (16).

The coefficient $C_2 = 2q - 1$ is not zero for $q \neq 1/2$. Thus, Eq. (16) is rewritten as follows:

$$\dot{v} = (K - \sqrt{\beta^2 - 1})v + (2q - 1)v^2 + O(v^3). \tag{25}$$

This equation corresponds to the normal form of a transcritical bifurcation described as $\dot{x} = \mu x \pm x^2$, because the magnitude of $v$ is relatively small. Thus, the stability of the two equilibrium points $(u, v) = (0, 0)$ and $(a_2 v_*^2, v_*)$, where

$$v_* = -\frac{K - \sqrt{\beta^2 - 1}}{2q - 1}, \tag{26}$$

changes at $K = \sqrt{\beta^2 - 1}$. By using Eqs. (13) and (14), the original trajectory of $(\phi_1, \phi_2)$ is described as follows:

$$\begin{aligned} \phi_1 &= u + 2qv + \phi_1^*, \\ \phi_2 &= u - 2(1 - q)v + \phi_2^*. \end{aligned} \tag{27}$$

We numerically confirmed that this approximation worked well near the bifurcation point as shown in Fig. 10. We note that the spontaneous oscillations do not emerge via this transcritical bifurcation. The spontaneous oscillation emerges via a SNIC bifurcation after the transcritical bifurcation as shown in Fig. 10.

## V. CONCLUSION AND DISCUSSION

We summarize the results of this paper and discuss future extensions. In this paper, we have analyzed the dynamical behavior of the system composed of coupled heterogeneous excitable units. Biological systems are often composed of a wide variety of heterogeneous excitable units. Therefore, the fascinating aspect of this problem is to investigate how this heterogeneity affects the collective behavior of the systems. Based on the bifurcation theory and the center manifold theory, we have elucidated how spontaneous oscillations emerge depending on the heterogeneity parameter and demonstrated three main results. First, we have clarified that the types of emergence of spontaneous oscillations are mainly determined by the order of occurrence of SNIC and heteroclinic bifurcations for an increase in the coupling strength. Second, we have found that when the system has symmetric properties, the mechanism of the oscillation emergence is analytically revealed as a 5th-order pitchfork bifurcation. Third, we have shown that the area of the parameter region corresponding to spontaneous oscillations decreases as the populations of the two groups become unbalanced.

The benefit of using a simple model is that the heterogeneity of excitable units is restricted only to the difference in the equilibrium states. Due to the simplicity of our model, we have clearly revealed the mechanism of spontaneous oscillations. Based on this basic understanding, further studies on the mechanism of heterogeneous excitable systems could be performed. There are various directions for future extension of this research, motivated by previous studies on dynamical systems, e.g., repulsive coupling among excitable elements [10], systems moving on a space [49], and systems whose coupling function contains phase shift [37,50]. Although various types of heterogeneity are found in real systems, our analysis of this basic model could be useful as a basis for understanding more complex systems. Therefore, from the perspective of dynamical systems, it is interesting to further investigate excitable systems in the future.

Finally, we will discuss the future extension of our study from the viewpoints of robustness and resilience. Our analysis suggests that heterogeneity of equilibrium states causes spontaneous oscillations in a system composed of excitable units. Because excitability plays an important role in biological systems such as the brain and heart, it is important to discern how the dynamical behavior of these systems maintains normal functions and recovers from possible damages. As we have introduced in Sec. I, the origin of oscillations is primarily attributable to active units in the networks composed of active and inactive units. On the other hand, for networks of heterogeneous excitable units, the origin of oscillations can be ascribed to excitable units. This suggests that the heterogeneity contributes to maintaining the dynamical behavior of the systems. In a system composed of excitable and passive units, the spontaneous oscillation occurs for sufficiently strong coupling strength [18]. Therefore, understanding of spontaneous

oscillations could be helpful in the investigation of the robustness of dynamical systems in the future. Moreover, this understanding could be also useful in the investigation of the effective recovery of the dynamical behavior of systems [36,51]. Thus, we believe that our work could be further developed from the perspective of dynamical systems and biological phenomena.

## ACKNOWLEDGMENTS

This research is partially supported by JSPS KAKENHI Grants No. JP26730127, No. JP15H05707, and No. JP17H05994, by the "Brain-Morphic AI to Resolve Social Issues" project, and by NEC Corporation.

## APPENDIX A: TWO SYMMETRIC PROPERTIES

We can find two symmetric properties in our system. Because of these symmetric properties, we can reduce the parameter region of $(\alpha, q)$ to be analyzed to $\{(\alpha, q) \mid \alpha \in [\pi/2, 3\pi/2], q \in [1/2, 1]\}$. Figure 11 is a graphical depiction of the parameter regions in the $(\alpha, q)$ plane. If we analyze the dynamical behavior of the parameter region $\{(\alpha, q) \mid \alpha \in [\pi/2, \pi], q \in [1/2, 1]\}$ which is marked with $A$, we can get those marked with $A_1$, $A_2$, and $A_{12}$ based on the following two symmetric properties. For the parameter region $\{(\alpha, q) \mid \alpha \in [\pi, 3\pi/2], q \in [1/2, 1]\}$ which is marked with $B$, we can get the dynamical behavior of the parameter regions $B_1$, $B_2$, and $B_{12}$ as in the case of the region $A$.

The first symmetric property is found around $\alpha = \pi$ and $q = 1/2$. Let us consider two trajectories generated from Eqs. (5) and (6) for $(\alpha, q) = (\alpha_1, q_1)$ and $(\hat{\alpha}_1, \hat{q}_1)$, which have the following relationship:

$$\hat{\alpha}_1 = 2\pi - \alpha_1, \quad \hat{q}_1 = 1 - q_1. \tag{A1}$$

To distinguish between these two trajectories, we denote the phase variables for the case of $(\hat{\alpha}_1, \hat{q}_1)$ by $(\hat{\phi}_1, \hat{\phi}_2)$. We also denote the corresponding frequencies defined in Eq. (7) by

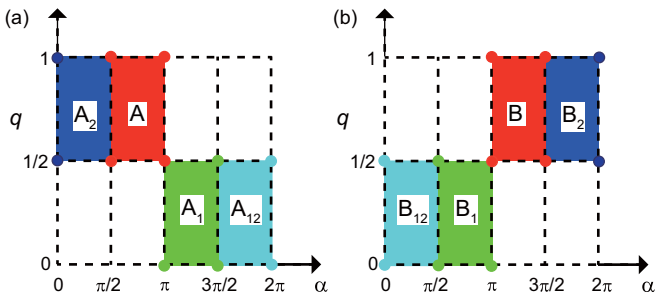


FIG. 11. Correspondence of the two symmetric properties in the parameter regions on the $(\alpha, q)$ plane analyzed in this paper. (a) The red parameter region $A$ ($\alpha \in [\pi/2, \pi]$ and $q \in [1/2, 1]$) corresponds to the regions $A_1$ and $A_2$ based on the first symmetric property in Eq. (A1) and the second one in Eq. (A7), respectively. The light-blue region $A_{12}$ corresponds to $A$ based on both symmetric properties. (b) The red parameter region $B$ ($\alpha \in [\pi, 3\pi/2]$ and $q \in [1/2, 1]$) corresponds to the regions $B_1$, $B_2$, and $B_{12}$ in the same way as (a).

$\hat{\Omega}_1$ and $\hat{\Omega}_2$, respectively. Then, the time evolution equations for $(\hat{\alpha}_1, \hat{q}_1)$ are given as follows:

$$\dot{\hat{\phi}}_1 = 1 - \beta \sin(\hat{\phi}_1) + \hat{q}_1 K \sin(\hat{\phi}_2 - \hat{\phi}_1), \tag{A2}$$

$$\dot{\hat{\phi}}_2 = 1 - \beta \sin(\hat{\phi}_2 + \hat{\alpha}_1) + (1 - \hat{q}_1) K \sin(\hat{\phi}_1 - \hat{\phi}_2). \tag{A3}$$

By substituting Eq. (A1) into these equations and exchanging the phase variables by

$$\hat{\phi}_1 = \phi_2 + \alpha_1 - 2\pi, \quad \hat{\phi}_2 = \phi_1 + \alpha_1 - 2\pi, \tag{A4}$$

we obtain the following equations:

$$\dot{\phi}_1 = 1 - \beta \sin(\phi_1) + q_1 K \sin(\phi_2 - \phi_1), \tag{A5}$$

$$\dot{\phi}_2 = 1 - \beta \sin(\phi_2 + \alpha_1) + (1 - q_1) K \sin(\phi_1 - \phi_2). \tag{A6}$$

These equations coincide with the original equations [Eqs. (5) and (6)] for $(\alpha, q) = (\alpha_1, q_1)$. Thus, the trajectory for the case of $(\alpha_1, q_1)$ can be understood by the trajectory for the case of $(\hat{\alpha}_1, \hat{q}_1)$ based on Eqs. (A1) and (A4), and vice versa. Moreover, the frequencies are also obtained based on Eq. (A4) as $\hat{\Omega}_1 = \Omega_2$ and $\hat{\Omega}_2 = \Omega_1$. Therefore, without loss of generality, we can restrict the parameter region to be analyzed. In Sec. III, we analyzed the emergence of the spontaneous oscillations for $\{(\alpha, q) \mid \alpha \in [\pi/2, \pi], q = 1/2\}$. From this result, we can obtain the trajectories for $\{(\alpha, q) \mid \alpha \in [\pi, 3\pi/2], q = 1/2\}$ based on Eq. (A1).

The second symmetric property is found around $\alpha = \pi/2$. Let us again consider two trajectories generated from Eqs. (5) and (6) for $(\alpha, q) = (\alpha_2, q_2)$ and $(\hat{\alpha}_2, q_2)$, which have the following relationship:

$$\hat{\alpha}_2 = \pi - \alpha_2. \tag{A7}$$

Then, the time evolution equations for $(\hat{\alpha}_2, q_2)$ are given as follows:

$$\dot{\hat{\phi}}_1 = 1 - \beta \sin(\hat{\phi}_1) + q_2 K \sin(\hat{\phi}_2 - \hat{\phi}_1), \tag{A8}$$

$$\dot{\hat{\phi}}_2 = 1 - \beta \sin(\hat{\phi}_2 + \hat{\alpha}_2) + (1 - q_2) K \sin(\hat{\phi}_1 - \hat{\phi}_2). \tag{A9}$$

By substituting Eq. (A7) into these equations and exchanging the phase and time variables by

$$\hat{\phi}_1 = -\phi_1 + \pi, \quad \hat{\phi}_2 = -\phi_2, \quad \tau = -t, \tag{A10}$$

we obtain the following equations:

$$\frac{d\phi_1}{d\tau} = 1 - \beta \sin(\phi_1) + q_2 K \sin(\phi_2 - \phi_1), \tag{A11}$$

$$\frac{d\phi_2}{d\tau} = 1 - \beta \sin(\phi_2 + \alpha_2) + (1 - q_2) K \sin(\phi_1 - \phi_2). \tag{A12}$$

These equations agree with the original equations for $(\alpha, q) = (\alpha_2, q_2)$ by getting it to go backward in time. Thus, the trajectories for the case of $(\alpha_2, q_2)$ can be understood by those for the case of $(\hat{\alpha}_2, q_2)$, and vice versa. Therefore, without loss of generality, we can restrict the parameter region to be analyzed. We note that the stability of the equilibrium points are different for the equations for $(\alpha_2, q_2)$ and for $(\hat{\alpha}_2, q_2)$. In Sec. III, the analyses for $\{(\alpha, q) \mid \alpha \in [\pi/2, \pi],$

$q = 1/2\}$ gave the trajectories for $\{(\alpha, q) \mid \alpha \in [0, \pi/2], q = 1/2\}$ based on Eq. (A7). Because the unstable equilibrium point remains with an increase in $K$ for $\alpha \in (\pi/2, \pi)$, the stable equilibrium point remains with an increase in $K$ for $\alpha \in (0, \pi/2)$. Thus, no spontaneous oscillations are observed in the region of $\alpha \in [0, \pi/2)$.

Based on these two symmetric properties, we should only focus on the region of $\{(\alpha, q) \mid \alpha \in [\pi/2, 3\pi/2], q \in [1/2, 1]\}$. The other cases of $(\alpha, q)$ can be understood according to the two symmetric properties as shown in Fig. 11.

## APPENDIX B: RELATIONSHIP TO OTHER STUDIES

Here, we show the relationship between our model in Eq. (2) and some models in related studies such as the Kuramoto model with external forcing [38–42], active rotators [43,44], and models of charge density wave (CDW) [45–47].

The Kuramoto model with external forcing is given by

$$\dot{\theta}_j = \omega_j + \frac{K}{N}\sum_{l=1}^{N}\sin(\theta_l - \theta_j) + M_j \sin(\Omega t + \alpha_j - \theta_j),$$
$$\text{for } j = 1, \ldots, N, \tag{B1}$$

where $M_j$ is the amplitude of the external forcing for the $j$th unit. By defining $\phi_j := \Omega t - \theta_j$, this equation can be written as follows:

$$\Omega - \dot{\phi}_j = \omega_j + \frac{K}{N}\sum_{l=1}^{N}\sin(\phi_j - \phi_l) + M_j \sin(\phi_j + \alpha_j). \tag{B2}$$

Then, we can derive

$$\dot{\phi}_j = (\Omega - \omega_j) - M_j \sin(\phi_j + \alpha_j) + \frac{K}{N}\sum_{l=1}^{N}\sin(\phi_l - \phi_j). \tag{B3}$$

This equation is similar to our model in Eq. (2). Thus, our study in this paper could provide insights into the Kuramoto model with heterogeneous external forcing.

An active rotator is a famous excitable model [43,44] that is often defined as follows:

$$\dot{\psi}_i = \omega - b\sin\psi_i + G_i(\psi_1, \ldots, \psi_N) + \xi_i(t),$$
$$\text{for } i = 1, \ldots, N, \tag{B4}$$

where $\psi_i$ represents the state variable of unit $i$, $G_i(\cdot)$ gives coupling functions among units $\{\psi_i\}$, and $\xi_i(t)$ is the Gaussian white random noise. Variants of this active rotator model have been investigated in many studies such as the effect of common noise on coupled active rotators [52]. The difference between active rotators and our model mainly lies in the following two points: the heterogeneity in the phase shift parameter $\alpha$ and the lack of noise effect in our model. Thus, our study that focuses on the effect of the heterogeneity of $\alpha$ could provide a new direction to the studies on active rotators.

The CDW model is defined as follows [45–47]:

$$\dot{\theta}_i = E - b\sin(\theta_i - \alpha_i) + \frac{K}{N}\sum_{j=1}^{N}\sin(\theta_j - \theta_i),$$
$$\text{for } i = 1, \ldots, N. \tag{B5}$$

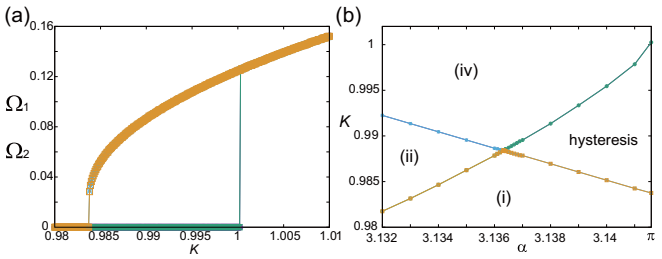


FIG. 12. (a) Dependencies of $\Omega_1$ and $\Omega_2$ on $K$ for $q = 1/2$ and $\alpha = \pi$. Green and yellow curves correspond to the cases of increasing and decreasing $K$, respectively. (b) The parameter region on the $(\alpha, K)$ plane is divided into four subregions around $\alpha = \pi$. Dynamics for regions (i), (ii), and (iv) correspond to those indicated in Fig. 2(a). A hysteresis region is found in the center-right part which is close to $\alpha = \pi$.

This model is almost the same as our model, but the distribution of $\alpha_i$ is different. Because Eq. (B5) was proposed as a CDW model, $\alpha_i$ was randomly determined from $[-\pi, \pi]$. In the previous studies, a hysteretic transition between non-oscillation and collective oscillation states was found in a part of the $(E, K)$ parameter plane [45–47]. In our setting, similarly, we found such hysteresis in a very small region on the $(\alpha, K)$ parameter plane for $q = 1/2$. As shown in Fig. 12(a), there is a parameter region for coexistence of a stable equilibrium point and an oscillating state which corresponds to $\Omega_1 = \Omega_2 = 0$ and $\Omega_1 = \Omega_2 > 0$, respectively. We show such a region on the $(\alpha, K)$ plane in Fig. 12(b). The hysteresis occurs in $(\alpha_h, \pi]$, where $\alpha_h \sim 3.13632$. The spontaneous oscillation individually emerges in $\alpha < \alpha_h$ as discussed in Sec. III. The similarity between the CDW model and our model is confirmed from this observation of hysteresis phenomena.

## APPENDIX C: ANALYSES BASED ON CENTER MANIFOLD THEORY

Here, we complement our analyses discussed in Sec. III D. The analyses were based on the center manifold theory. See [48] for a detailed introduction to this theory. We have analyzed the stability changes of the stable equilibrium point. For $\alpha = \pi$, as we have discussed in Sec. III D, Eqs. (5) and (6) have an equilibrium point $(\phi_1^*, \phi_2^*) = (\arcsin(1/\beta), \arcsin(1/\beta) + \pi)$. We denote the displacement from the equilibrium point by $(\psi_1, \psi_2)$, i.e., $\phi_1 = \psi_1 + \phi_1^*$ and $\phi_2 = \psi_2 + \phi_2^*$. By substituting these equations into Eqs. (5) and (6), the time expansion equations of the displacement variables $(\psi_1, \psi_2)$ are given as follows:

$$\dot{\psi}_1 = 1 - \beta\sin(\psi_1 + \phi_1^*) + qK\sin(\psi_2 + \phi_2^* - \psi_1 - \phi_1^*), \tag{C1}$$

$$\dot{\psi}_2 = 1 - \beta\sin(\psi_2 + \phi_2^* + \pi) + K(1-q)\sin(\psi_1 + \phi_1^* - \psi_2 - \phi_2^*). \tag{C2}$$

By taking Taylor expansion of Eq. (C1), we obtain its polynomial expression as follows:

$$\begin{aligned}\dot{\psi}_1 &= 1-\beta\big[\sin(\phi_1^*)+\cos(\phi_1^*)\psi_1+H_1^{(2)}(\psi_1)\big]\\ &\quad+qK\big[\sin(\phi_2^*-\phi_1^*)+\cos(\phi_2^*-\phi_1^*)(\psi_2-\psi_1)\\ &\quad+H_3^{(2)}(\psi_1,\psi_2)\big]\\ &=(qK-\sqrt{\beta^2-1})\psi_1-qK\psi_2\\ &\quad-\beta H_1^{(2)}(\psi_1)+qKH_3^{(2)}(\psi_1,\psi_2),\end{aligned}\tag{C3}$$

where $H_1^{(2)}$ is the nonlinear polynomial terms of $\sin(\psi_1+\phi_1^*)$ as follows:

$$H_1^{(2)}(\psi_1)=\lim_{M\to\infty}\sum_{k=2}^{M}\left.\frac{d^k\sin(x)}{dx^k}\right|_{x=\phi_1^*}\frac{(\psi_1)^k}{k!},\tag{C4}$$

and $H_3^{(2)}$ is that of $\sin(\psi_2+\phi_2^*-\psi_1-\phi_1^*)$ as follows:

$$H_3^{(2)}(\psi_1,\psi_2)=\lim_{M\to\infty}\sum_{k=2}^{M}\left.\frac{d^k\sin(x)}{dx^k}\right|_{x=\phi_2^*-\phi_1^*}\frac{(\psi_2-\psi_1)^k}{k!}.\tag{C5}$$

We also take Taylor expansion of Eq. (C2) and obtain its polynomial expression as follows:

$$\begin{aligned}\dot{\psi}_2 &= 1+\beta\big[\sin(\phi_2^*)+\cos(\phi_2^*)\psi_2+H_2^{(2)}(\psi_2)\big]\\ &\quad-K(1-q)\big[\sin(\phi_2^*-\phi_1^*)+\cos(\phi_2^*-\phi_1^*)(\psi_2-\psi_1)\\ &\quad+H_3^{(2)}(\psi_1,\psi_2)\big]\\ &=-K(1-q)\psi_1+(K(1-q)-\sqrt{\beta^2-1})\psi_2\\ &\quad+\beta H_2^{(2)}(\psi_2)-K(1-q)H_3^{(2)}(\psi_1,\psi_2),\end{aligned}\tag{C6}$$

where $H_2^{(2)}$ is the nonlinear polynomial terms of $\sin(\psi_2+\phi_2^*)$ as follows:

$$H_2^{(2)}(\psi_2)=\lim_{M\to\infty}\sum_{k=2}^{M}\left.\frac{d^k\sin(x)}{dx^k}\right|_{x=\phi_2^*}\frac{1}{k!}(\psi_2)^k.\tag{C7}$$

From Eqs. (C3) and (C6), we can rewrite Eqs. (C1) and (C2) as follows:

$$\begin{pmatrix}\dot{\psi}_1\\ \dot{\psi}_2\end{pmatrix}=A\begin{pmatrix}\psi_1\\ \psi_2\end{pmatrix}+\begin{pmatrix}-\beta H_1^{(2)}(\psi_1)+KqH_3^{(2)}(\psi_1,\psi_2)\\ \beta H_2^{(2)}(\psi_2)-K(1-q)H_3^{(2)}(\psi_1,\psi_2)\end{pmatrix},\tag{C8}$$

where

$$A=\begin{pmatrix}-\sqrt{\beta^2-1}+Kq & -Kq\\ -K(1-q) & -\sqrt{\beta^2-1}+K(1-q)\end{pmatrix}.\tag{C9}$$

The two eigenvalues of $A$ are $\lambda_K:=K-\sqrt{\beta^2-1}$ and $\lambda_0:=-\sqrt{\beta^2-1}<0$ and their corresponding eigenvectors are $\mathbf{e}_K=2(q,q-1)^\top$ and $\mathbf{e}_0=(1,1)^\top$, respectively. We transform the variables $(\psi_1,\psi_2)$ into $(u,v)$ as follows:

$$\begin{pmatrix}\psi_1\\ \psi_2\end{pmatrix}=u\,\mathbf{e}_0+v\,\mathbf{e}_K,\tag{C10}$$

which gives

$$\begin{pmatrix}u\\ v\end{pmatrix}=(\mathbf{e}_0\quad\mathbf{e}_K)^{-1}\begin{pmatrix}\psi_1\\ \psi_2\end{pmatrix}.\tag{C11}$$

Then, we obtain the following relationships:

$$u=(1-q)\psi_1+q\psi_2,\tag{C12}$$

$$v=\frac{\psi_1-\psi_2}{2}.\tag{C13}$$

Note that $\psi_1$ and $\psi_2$ are functions of $u$ and $v$. Then, we get the time derivative of $u$ as follows:

$$\dot{u}=(1-q)\dot{\psi}_1+q\dot{\psi}_2=Gu+h_u(u,v),\tag{C14}$$

where

$$\begin{aligned}G&:=-\sqrt{\beta^2-1},\\ h_u(u,v)&:=-\beta(1-q)H_1^{(2)}(\psi_1(u,v))+\beta qH_2^{(2)}(\psi_2(u,v)).\end{aligned}\tag{C15}$$

Also, we get the time derivative of $v$ as follows:

$$\dot{v}=\frac{\dot{\psi}_1-\dot{\psi}_2}{2}=B_Kv+h_v(u,v),\tag{C16}$$

where

$$\begin{aligned}B_K&:=K-\sqrt{\beta^2-1},\\ h_v(u,v)&:=-\frac{\beta}{2}H_1^{(2)}(\psi_1(u,v))-\frac{\beta}{2}H_2^{(2)}(\psi_2(u,v))\\ &\quad+\frac{K}{2}H_3^{(2)}(\psi_1(u,v),\psi_2(u,v)).\end{aligned}$$

Equation (C16) gives the dynamics on the center manifold. According to the center manifold theory [48], $u$ can be written as a function of $v$ as follows:

$$u=m(v):=\sum_{k\geqslant 2}a_kv^k.\tag{C17}$$

Thus, we can derive the dynamics on the center manifold as a function of only $v$ by acquiring the coefficients $a_k$.

Next, we obtain these coefficients based on the center manifold theory [48]. From Eqs. (C16) and (C17), the time derivative of $u$ is obtained as

$$\dot{u}=\frac{dm(v)}{dv}\dot{v}=\frac{dm(v)}{dv}[B_Kv+h_v(u,v)].\tag{C18}$$

This must be the same as Eq. (C14), and therefore, an identical equation is obtained as follows:

$$[B_Kv+h_v(m(v),v)]\frac{dm(v)}{dv}=[Gm(v)+h_u(m(v),v)].\tag{C19}$$

By comparing the coefficients of each order of $v$ of this equation, we can obtain the coefficients $a_k$. To do this, we rewrite the terms of $H_1^{(2)}(\psi_1(u,v))$, $H_2^{(2)}(\psi_2(u,v))$, and $H_3^{(2)}(\psi_1(u,v),\psi_2(u,v))$ as direct functions of $u$ and $v$. From Eqs. (C12) and (C13), $\psi_1$ and $\psi_2$ can be rewritten as follows:

$$\begin{aligned}\psi_1&=u+2qv,\\ \psi_2&=u-2(1-q)v.\end{aligned}\tag{C20}$$

By substituting these relationships into Eqs. (C4), (C5), and (C7), we obtain

$$\begin{aligned} &H_1^{(2)}(\psi_1(u,v)) \\ &= \lim_{M\to\infty}\sum_{k=2}^{M}\left.\frac{d^k\sin(x)}{dx^k}\right|_{x=\phi_1^*}\frac{1}{k!}\psi_1^k \\ &= \lim_{M\to\infty}\sum_{k=2}^{M}\left.\frac{d^k\sin(x)}{dx^k}\right|_{x=\phi_1^*}\frac{1}{k!}(u+2qv)^k \\ &= \lim_{M\to\infty}\sum_{k=2}^{M}\left.\frac{d^k\sin(x)}{dx^k}\right|_{x=\phi_1^*}\frac{1}{k!}\left(\sum_{l=2}^{N}a_l v^l+2qv\right)^k, \end{aligned} \tag{C21}$$

$$\begin{aligned} &H_2^{(2)}(\psi_2(u,v)) \\ &= \lim_{M\to\infty}\sum_{k=2}^{M}\left.\frac{d^k\sin(x)}{dx^k}\right|_{x=\phi_2^*}\frac{1}{k!}\psi_2^k \\ &= \lim_{M\to\infty}\sum_{k=2}^{M}\left.\frac{d^k\sin(x)}{dx^k}\right|_{x=\phi_2^*}\frac{1}{k!}[u-2(1-q)v]^k \\ &= \lim_{M\to\infty}\sum_{k=2}^{M}\left.\frac{d^k\sin(x)}{dx^k}\right|_{x=\phi_2^*}\frac{1}{k!}\left[\sum_{l=2}^{N}a_l v^l-2(1-q)v\right]^k, \end{aligned} \tag{C22}$$

and

$$\begin{aligned} &H_3^{(2)}(\psi_1(u,v),\psi_2(u,v)) \\ &= \lim_{M\to\infty}\sum_{k=2}^{M}\left.\frac{d^k\sin(x)}{dx^k}\right|_{x=\phi_2^*-\phi_1^*}\frac{1}{k!}(\psi_2-\psi_1)^k \\ &= \lim_{M\to\infty}\sum_{k=2}^{M}\left.\frac{d^k\sin(x)}{dx^k}\right|_{x=\pi}\frac{1}{k!}(-2v)^k. \end{aligned} \tag{C23}$$

Hereafter, we denote these terms by $H_1^{(2)}(u,v)$, $H_2^{(2)}(u,v)$, and $H_3^{(2)}(u,v)$, respectively. By substituting the aforementioned conditions of our problem under consideration, we rewrite Eq. (C19) as follows:

$$\begin{aligned} &\left[(K-\sqrt{\beta^2-1})v-\frac{\beta}{2}H_1^{(2)}(u,v)-\frac{\beta}{2}H_2^{(2)}(u,v)\right. \\ &\left.+\frac{K}{2}H_3^{(2)}(u,v)\right]\sum_{k\geqslant 2}ka_k v^{k-1}-\left[-\sqrt{\beta^2-1}\sum_{k\geqslant 2}a_k v^k\right. \\ &\left.-\beta(1-q)H_1^{(2)}(u,v)+\beta q H_2^{(2)}(u,v)\right]=0. \end{aligned} \tag{C24}$$

We have analyzed the orders of $v^2$, $v^3$, $v^4$, and $v^5$ in this study. For these cases, the former parts of Eq. (C21) are obtained as follows:

$$\left.\frac{d^2\sin(x)}{dx^2}\right|_{x=\phi_1^*}\frac{1}{2!}=-\frac{\sin(\phi_1^*)}{2}=-\frac{1}{2\beta},$$

$$\left.\frac{d^3\sin(x)}{dx^3}\right|_{x=\phi_1^*}\frac{1}{3!}=-\frac{\cos(\phi_1^*)}{6}=-\frac{\sqrt{\beta^2-1}}{6\beta},$$

$$\left.\frac{d^4\sin(x)}{dx^4}\right|_{x=\phi_1^*}\frac{1}{4!}=\frac{\sin(\phi_1^*)}{24}=\frac{1}{24\beta},$$

$$\left.\frac{d^5\sin(x)}{dx^5}\right|_{x=\phi_1^*}\frac{1}{5!}=\frac{\cos(\phi_1^*)}{120}=\frac{\sqrt{\beta^2-1}}{120\beta}.$$

Because $\sin(\phi_2^*)=\sin(\phi_1^*+\pi)=-\sin(\phi_1^*)$ and $\cos(\phi_2^*)=\cos(\phi_1^*+\pi)=-\cos(\phi_1^*)$, we get the former parts of Eq. (C22) by changing the signs of the corresponding parts of Eq. (C21). In the case of Eq. (C23), we obtain

$$\left.\frac{d^2\sin(x)}{dx^2}\right|_{x=\pi}\frac{1}{2!}(-2v)^2=-\frac{\sin(\pi)}{2}4v^2=0,$$

$$\left.\frac{d^3\sin(x)}{dx^3}\right|_{x=\pi}\frac{1}{3!}(-2v)^3=-\frac{\cos(\pi)}{6}(-8v^3)=-\frac{8}{6}v^3,$$

$$\left.\frac{d^4\sin(x)}{dx^4}\right|_{x=\pi}\frac{1}{4!}(-2v)^4=\frac{\sin(\pi)}{24}(16v^4)=0,$$

$$\left.\frac{d^5\sin(x)}{dx^5}\right|_{x=\pi}\frac{1}{5!}(-2v)^5=\frac{\cos(\pi)}{120}(-32v^5)=\frac{32}{120}v^5.$$

By substituting these coefficients into Eq. (C24), we obtain the coefficients $a_k$. As for $v^2$, the corresponding part of Eq. (C24) is given by

$$\begin{aligned} &[(K-\sqrt{\beta^2-1})v]2a_2v-\left[-\sqrt{\beta^2-1}a_2v^2\right. \\ &\left.-\beta(1-q)\left(-\frac{4q^2v^2}{2\beta}\right)+\beta q\frac{4(1-q)^2v^2}{2\beta}\right]=0. \end{aligned} \tag{C25}$$

The coefficient of $v^2$ is given by

$$2(K-\sqrt{\beta^2-1})a_2+\sqrt{\beta^2-1}a_2-2(1-q)q^2-2q(1-q)^2. \tag{C26}$$

This coefficient must be zero, and thus, the first coefficient $a_2$ is obtained as follows:

$$a_2=\frac{2q(1-q)}{2K-\sqrt{\beta^2-1}}. \tag{C27}$$

Other coefficients of $a_3$ and $a_4$ are obtained in a similar way as follows:

$$a_3=0, \tag{C28}$$

$$a_4=-\frac{-28K^2+8K\sqrt{\beta^2-1}+3\beta^2+6}{24(2K-\sqrt{\beta^2-1})^2(4K-3\sqrt{\beta^2-1})}. \tag{C29}$$

We note that $q=1/2$ is assumed for this derivation. Therefore, from Eq. (C16), we can derive the dynamics on the center manifold as follows:

$$\dot{v}=B_K v+h_v\left(\sum_{k\geqslant 2}a_k v^k, v\right). \tag{C30}$$

Finally, we check how the bifurcation types depend on the parameters. Because the second term of Eq. (C30) is a polynomial expression of $v$, we express the equation as follows:

$$\dot{v}=B_K v+\sum_{k\geqslant 2}C_k v^k. \tag{C31}$$

We can determine $C_k$ by substituting the obtained coefficients $a_k$ into Eq. (C30). The first coefficient $C_2$ is given by

$$C_2 = 2q - 1. \tag{C32}$$

If $q \neq 1/2$, this indicates that the dynamics on the center manifold can be approximated as follows:

$$\dot{v} = (K - \sqrt{\beta^2 - 1})v + (2q - 1)v^2, \tag{C33}$$

because the magnitude of $v$ is relatively small. This equation corresponds to the normal form of a transcritical bifurcation, $\dot{x} = \mu x \pm x^2$, as discussed in Sec. IV B. For $q = 1/2$, the coefficient $C_2$ is equal to zero. In this case, we need to investigate higher order terms. Thus, the equation is rewritten as follows:

$$\dot{v} = (K - \sqrt{\beta^2 - 1})v + C_3 v^3, \tag{C34}$$

where

$$C_3 = \frac{3 + (-4K + \sqrt{\beta^2 - 1})(2K - \sqrt{\beta^2 - 1})}{6(2K - \sqrt{\beta^2 - 1})}.$$

At the critical point $K_* = \sqrt{\beta^2 - 1}$, the coefficient $C_3$ is rewritten as follows:

$$C_3 = \frac{2 - \beta^2}{2\sqrt{\beta^2 - 1}}.$$

When $C_3 \neq 0$ ($\beta \neq \sqrt{2}$), Eq. (C34) indicates the pitchfork bifurcation at $K = \sqrt{\beta^2 - 1}$, supercritical pitchfork bifurcation for $C_3 < 0$ ($\beta > \sqrt{2}$) and subcritical pitchfork bifurcation for $C_3 > 0$ ($\beta < \sqrt{2}$). Especially when $q = 1/2$ and $\beta = \sqrt{2}$, both the coefficients $C_2$ and $C_3$ are equal to zero. In this case, we need to investigate much higher order terms. Thus, the equation is rewritten again as

$$\dot{v} = (K - \sqrt{\beta^2 - 1})v + C_5 v^5, \tag{C35}$$

where

$$\begin{aligned} C_5 = &\frac{1}{120(2K - \sqrt{\beta^2 - 1})^2(4K - 3\sqrt{\beta^2 - 1})}[-15(\beta^2 + 2) \\ &+ 15(2K - \sqrt{\beta^2 - 1})(2K + 5\sqrt{\beta^2 - 1}) \\ &+ (16K - \sqrt{\beta^2 - 1})(2K - \sqrt{\beta^2 - 1})^2(4K \\ &- 3\sqrt{\beta^2 - 1})]. \end{aligned}$$

Note that $C_4 = 0$. Because we now consider the case of $\beta = \sqrt{2}$, $C_5$ can be rewritten as follows:

$$C_5 = \frac{\beta^4 + 4\beta^2 - 8}{8(\beta^2 - 1)\sqrt{\beta^2 - 1}} = \frac{4 + 4 \times 2 - 8}{8(2 - 1)\sqrt{2 - 1}} = \frac{1}{2}. \tag{C36}$$

Therefore, the system shows a 5th-order pitchfork bifurcation at $K = K_*$. As discussed in this appendix, we can determine the bifurcation types based on the center manifold theory.


[1] D. Pazó and E. Montbrió, Phys. Rev. E **73**, 055202 (2006).
[2] H. Daido, A. Kasama, and K. Nishio, Phys. Rev. E **88**, 052907 (2013).
[3] H. Daido, Phys. Rev. E **96**, 012210 (2017).
[4] H. Daido and K. Nishio, Phys. Rev. E **93**, 052226 (2016).
[5] A. Hjelmfelt and J. Ross, Proc. Natl. Acad. Sci. USA **91**, 63 (1994).
[6] C. R. Laing, Phys. Rev. E **90**, 010901 (2014).
[7] D. Taylor and P. Holmes, J. Math. Biol. **37**, 419 (1998).
[8] L. M. Alonso and G. B. Mindlin, Chaos **21**, 023102 (2011).
[9] L. M. Alonso, Chaos **27**, 063104 (2017).
[10] M. A. Zaks and P. Tomov, Phys. Rev. E **93**, 020201 (2016).
[11] S. A. Plotnikov, J. Lehnert, A. L. Fradkov, and E. Schöll, Phys. Rev. E **94**, 012203 (2016).
[12] M. C. Cross and P. C. Hohenberg, Rev. Mod. Phys. **65**, 851 (1993).
[13] J. J. Tyson and J. P. Keener, Phys. D (Amsterdam, Neth.) **32**, 327 (1988).
[14] B. Van der Pol and J. Van Der Mark, Nature (London) **120**, 363 (1927).
[15] R. FitzHugh, Biophys. J. **1**, 445 (1961).
[16] J. Nagumo, S. Arimoto, and S. Yoshizawa, Proc. IRE **50**, 2061 (1962).
[17] B. Ermentrout, Neural Comput. **8**, 979 (1996).
[18] A. Kryukov, V. Petrov, L. Averyanova, G. Osipov, W. Chen, O. Drugova, and C. Chan, Chaos **18**, 037129 (2008).
[19] Y. Kuramoto, *Chemical Oscillations, Waves, and Turbulence* (Springer, New York, 1984).
[20] A. T. Winfree, *The Geometry of Biological Time* (Springer Science & Business Media, New York, 2001).
[21] A. Pikovsky, M. Rosenblum, and J. Kurths, *Synchronization: A Universal Concept in Nonlinear Sciences* (Cambridge University Press, Cambridge, 2001).
[22] J. A. Acebrón, L. L. Bonilla, C. J. Pérez Vicente, F. Ritort, and R. Spigler, Rev. Mod. Phys. **77**, 137 (2005).
[23] H. Daido and K. Nakanishi, Phys. Rev. Lett. **93**, 104101 (2004).
[24] G. Tanaka, Y. Okada, and K. Aihara, Phys. Rev. E **82**, 035202 (2010).
[25] G. Tanaka, K. Morino, and K. Aihara, Sci. Rep. **2**, 232 (2012).
[26] G. Tanaka, K. Morino, and K. Aihara, in *Mathematical Approaches to Biological Systems*, edited by T. Ohira and T. Uzawa (Springer, Tokyo, 2015), pp. 29–53.
[27] K. Morino, G. Tanaka, and K. Aihara, Phys. Rev. E **83**, 056208 (2011).
[28] T. Sasai, K. Morino, G. Tanaka, J. A. Almendral, and K. Aihara, PLoS ONE **10**, e0123722 (2015).
[29] T. Yuan, K. Aihara, and G. Tanaka, Phys. Rev. E **95**, 012315 (2017).
[30] W. Huang, X. Zhang, X. Hu, Y. Zou, Z. Liu, and S. Guan, Chaos **24**, 023122 (2014).
[31] G. Tanaka, K. Morino, H. Daido, and K. Aihara, Phys. Rev. E **89**, 052906 (2014).
[32] H. Daido, Phys. Rev. E **84**, 016215 (2011).
[33] B. Thakur, D. Sharma, and A. Sen, Phys. Rev. E **90**, 042904 (2014).

[34] K. P. O'Keeffe and S. H. Strogatz, Phys. Rev. E **93**, 062203 (2016).
[35] T. Yuan and G. Tanaka, Chaos **27**, 123105 (2017).
[36] K. Morino, G. Tanaka, and K. Aihara, Phys. Rev. E **88**, 032909 (2013).
[37] H. Sakaguchi and Y. Kuramoto, Prog. Theor. Phys. **76**, 576 (1986).
[38] H. Sakaguchi, Prog. Theor. Phys. **79**, 39 (1988).
[39] L. F. Lafuerza, P. Colet, and R. Toral, Phys. Rev. Lett. **105**, 084101 (2010).
[40] E. Ott and T. M. Antonsen, Chaos **18**, 037113 (2008).
[41] L. M. Childs and S. H. Strogatz, Chaos **18**, 043128 (2008).
[42] T. Antonsen Jr., R. Faghih, M. Girvan, E. Ott, and J. Platig, Chaos **18**, 037112 (2008).
[43] S. Shinomoto and Y. Kuramoto, Prog. Theor. Phys. **75**, 1105 (1986).
[44] S. Shinomoto and Y. Kuramoto, Prog. Theor. Phys. **75**, 1319 (1986).
[45] S. H. Strogatz, C. M. Marcus, R. M. Westervelt, and R. E. Mirollo, Phys. Rev. Lett. **61**, 2380 (1988).
[46] S. H. Strogatz, C. M. Marcus, R. M. Westervelt, and R. E. Mirollo, Phys. D (Amsterdam, Neth.) **36**, 23 (1989).
[47] C. M. Marcus, S. H. Strogatz, and R. M. Westervelt, Phys. Rev. B **40**, 5588 (1989).
[48] Y. A. Kuznetsov, *Elements of Applied Bifurcation Theory* (Springer Science & Business Media, New York, 2013).
[49] N. Fujiwara, J. Kurths, and A. Díaz-Guilera, Phys. Rev. E **83**, 025101(R) (2011).
[50] T. Aoki and T. Aoyagi, Phys. Rev. Lett. **102**, 034101 (2009).
[51] W. Zou, D. V. Senthilkumar, R. Nagao, I. Z. Kiss, Y. Tang, A. Koseska, J. Duan, and J. Kurths, Nat. Commun. **6**, 7709 (2015).
[52] A. V. Dolmatova, D. S. Goldobin, and A. Pikovsky, Phys. Rev. E **96**, 062204 (2017).